Mon. Not. R. astr. Soc. (1980) **193**, 427–437

Observations of M87 at 15.4 GHz with the 5-km telescope

R. A. Laing★ *Mullard Radio Astronomy Observatory, Cavendish Laboratory, Madingley Road, Cambridge CB3 0HE*

Received 1980 March 21; in original form 1980 February 5

Summary. The radio galaxy M87 has been mapped with a resolution of 0.67 × 2.1 arcsec^2 using the Cambridge 5-km telescope at a frequency of 15.4 GHz. The radio jet consists of discrete knots separated by regions of low surface brightness within ~ 20 arcsec of the nucleus, but merges into a diffuse ridge of emission at larger distances. The jet appears to oscillate from side to side with an amplitude which increases with increasing distance from the nucleus; observations of the linearly-polarized emission show that the magnetic field within the jet is well-ordered and aligned with its axis.

1 Introduction

The giant elliptical galaxy M87 is associated with the radio source Virgo A (3C 274) and has long been famous for its optical jet. Work on this radio source was reviewed by Turland (1975), who also presented a map made at 5.0 GHz with the 5-km telescope (HPBW = 2 × 9 arcsec^2); more recent radio observations were made by Forster *et al.* (1978) using the Berkeley interferometer at 23 GHz (HPBW = 6 × 10 arcsec^2). The optical polarization of the jet was most recently measured by Schmidt, Peterson & Beaver (1978) and detailed photometry has been presented by de Vaucouleurs & Nieto (1979; hereafter VN).

The purpose of this paper is to describe observations of M87 made at 15.4 GHz with the 5-km telescope. At this frequency and resolution, the extended halo (e.g. Andernach *et al.* 1979; Kotanyi 1980) is not detected and the following discussion refers only to the core source, whose dimensions are ~ 40 arcsec by ~ 60 arcsec. The principal objectives are:

(a) To study the brightness distribution along the jet at high resolution.

(b) To map the linearly-polarized emission from the jet and to derive the structure of the magnetic field within it.

A discussion of the spectrum, Faraday rotation and depolarization of the source on the basis of maps made at 2.7, 5.0, 15.4 and 23 GHz will be presented elsewhere.

In Section 2, the observations and their subsequent reduction are briefly described. The brightness distributions of the extended emission and of the jet are presented in Sections

★ Present address: National Radio Astronomy Observatory, Edgemont Road, Charlottesville, Virginia 22901, USA.

3.1 and 3.2 respectively and the polarization properties of the jet are discussed in Section 4. The main conclusions are summarized in Section 5.

The distance to M87 is assumed to be 20 Mpc. This value is derived from the mean velocity of the Virgo cluster ellipticals, assuming a Hubble constant of $H_0 = 50\,\mathrm{km\,s^{-1}\,Mpc^{-1}}$. One arcsec therefore corresponds to 100 pc. All positions quoted are for epoch 1950.0.

2 Observations and data reduction

M87 was observed with the Cambridge 5-km telescope in the Stokes parameters $I + Q$ at 15.375 GHz in two 12-hr observations at each of four positions of the moving aerials, giving a total of 64 interferometer spacings. The nearby unresolved source 1252 + 119 was used as a phase calibrator, as described by Riley & Pooley (1978). The resolution of the 5-km telescope at 15.4 GHz is 0.67 arcsec in RA and the grating ring radius is $14(N/16)$ arcsec, where N is the number of interferometer spacings. Both these values are increased by a factor of cosec δ in declination. M87 is at a declination of 12° 40′ so that its elevation was very low at the beginnings and ends of the observations. The map made with the raw phases was therefore badly disfigured by the effects of tropospheric phase irregularities, but the nuclear source is bright enough to be used as a phase reference and is also unresolved. The main effect of tropospheric irregularities is to produce linear phase gradients, which correspond to shifts in the position of the source. The technique adopted to reduce their effects was to derive a one-dimensional Fourier transform of a single one-minute sample of the visibility function, and to locate the peak of the transform (which corresponded to the nuclear source). An appropriate phase gradient was then introduced to move the peak to an assumed map-centre position, hence cancelling out the effects of the atmosphere to first order, and a map was synthesized using the corrected phases. The method broke down over the small range of hour angle for which the peaks in the Fourier transform corresponding to the nuclear source and the jet overlapped, and this produced a weak spurious feature on the opposite side of the nucleus to the jet which could, however, easily be recognized as such and ignored. Absolute positional information is lost if a phase-referencing technique of this type is used and all positions are determined relative to that of the central source, which was assumed to be $\alpha = 12^{\mathrm{h}}\,28^{\mathrm{m}}\,17^{\mathrm{s}}.556$, $\delta = 12°\,40'\,02''.0$ (Turland 1975).

Two independent observations of the Stokes parameters U and Q were made in order to derive the distribution of linearly-polarized intensity; these were made with the same configuration of the moving aerials and cover the region of the jet only. The phase-referencing technique was not used. There are no spurious sidelobes from the nuclear source, which is essentially unpolarized, on the maps of U and Q; the effects of tropospheric phase errors are therefore small compared with those on the map of $I + Q$. No corrections have been made for instrumental polarization, which is less than 0.1 per cent. Any positional discrepancies between the maps of $I + Q$ and those of U and Q introduced by the phase-referencing method are less than 0.1 arcsec in RA and 0.5 arcsec in Dec.

The flux-density scale was based on a value of $I = 3.38$ Jy for 3C 286 (derived from Genzel *et al.* 1976, with a small correction for the frequency difference). This source was assumed to be 11.1 per cent polarized in PA 32°.5 at 15.4 GHz (Tabara & Inoue 1980).

3 The brightness distribution

3.1 THE OVERALL STRUCTURE

Fig. 1 shows a contour map of M87 in the Stokes parameters $I + Q$. There are three main components: a bright ($I = 3.1 \pm 0.2$ Jy) unresolved central core, a diffuse eastern lobe with

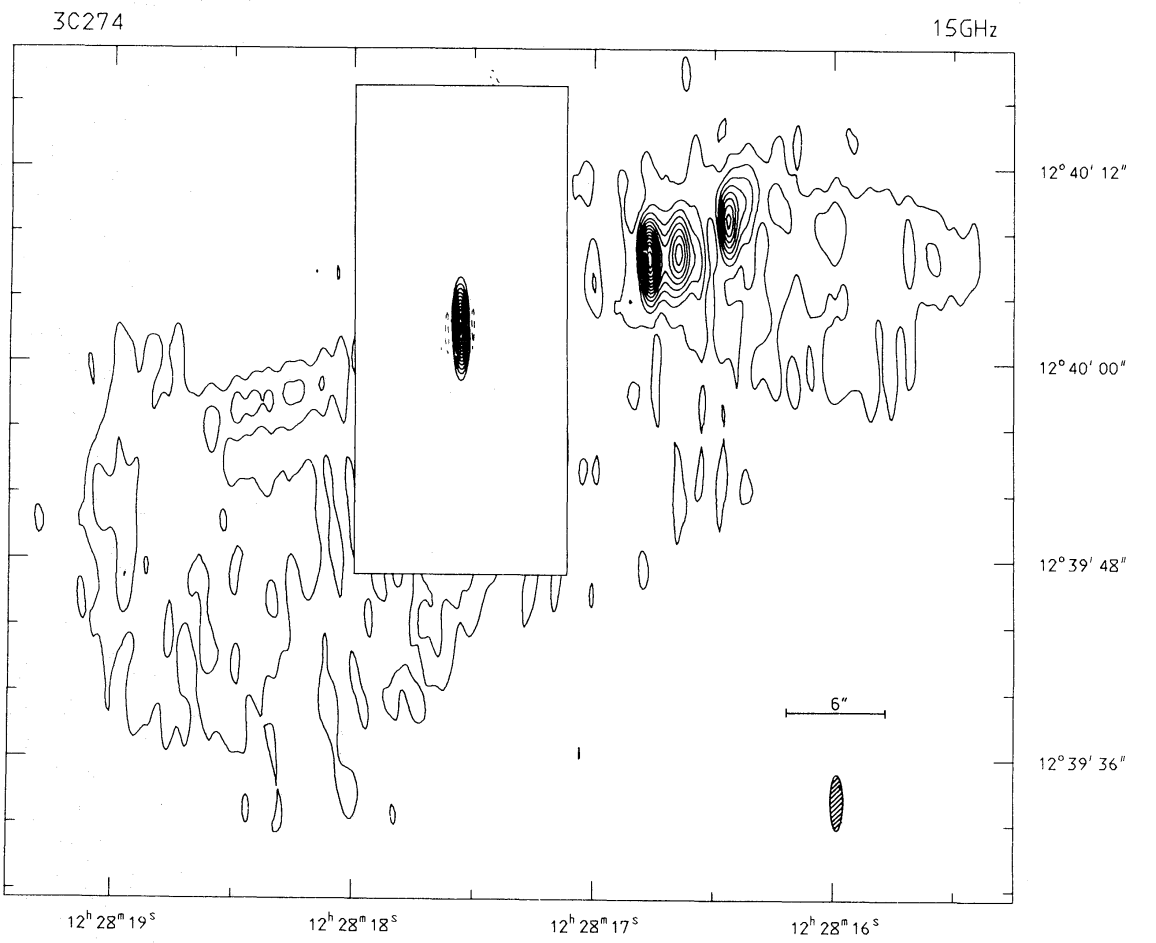

Figure 1. A contour map of M87 in the Stokes parameters $I + Q$. The contour intervals are 260 mJy and 26 mJy respectively in the central and outer panels.

no appreciable structure on a scale of < 2 arcsec, and, to the west, a curved, knotty jet superimposed on more extended emission. The central panel of Fig. 1 is affected by irregular sidelobes of the bright central component caused by residual phase errors, and a high contour level has therefore been used.

The source is roughly triangular in outline, narrowing towards the west. Both the nucleus and the jet are on the northern edge of the source, although there is some extended emission to the north of the jet. The apparent 'counter-jet' between right ascensions $12^h\,28^m\,18^s.0$ and $18^s.5$ in the eastern lobe is an artefact of the phase-referencing method. The slight enhancement of emission at the eastern edge of the source is also visible on the maps of Turland (1975) and Forster *et al.* (1978) and is likely to be real.

3.2 THE JET

The aim of this section is to answer the following questions:

(a) Does the jet consist of discrete sources only, or is it a continuous stream with local enhancements of emission?

(b) What are the flux densities, positions and sizes of any discrete components?

(c) How well are the knots aligned with the central source?

(d) What is the relationship between the optical and radio structures?

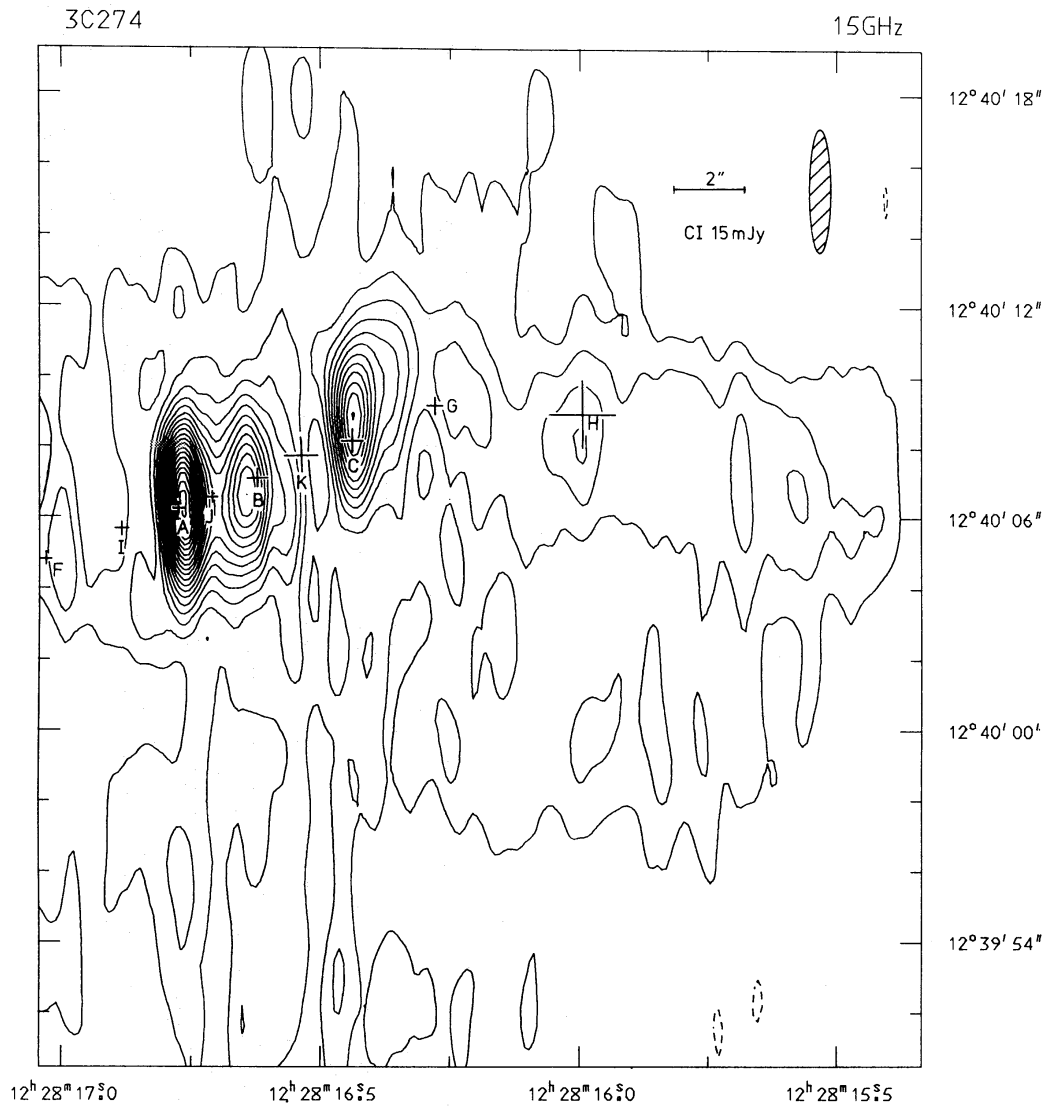

Figure 2. A contour map of the western lobe of M87 in the Stokes parameter I (total intensity). The positions of the optical knots listed by VN are marked by crosses; the arms of a cross represent 1σ errors.

A contour map of the western lobe in the Stokes parameter I is shown in Fig. 2; the positions of the optical knots listed by VN are marked by crosses. When referring to individual knots, the notation of VN will be used (see Fig. 2).

The radio brightness distribution along the jet is complex; the knots are resolved and are superimposed on a ridge of emission which continues to the western tip of the source. Peaks in the radio emission are detected at the positions of the optical knots F, A, B, C, G and H; a brightness profile along the crest of the jet is shown in Fig. 3, and the optical and radio parameters of the knots are listed in Table 1 as follows:

Column 1: Name (from VN)

Columns 2, 3 and 4: Coordinates of the peaks of emission, with estimated errors. The optical positions were taken from VN.

Column 5: The size of the knot along the axis of the jet, as estimated from the radio brightness profiles of Fig. 3. The quoted sizes are FWHM, assuming a Gaussian brightness profile; this is obviously a crude approximation for the better-resolved knots.

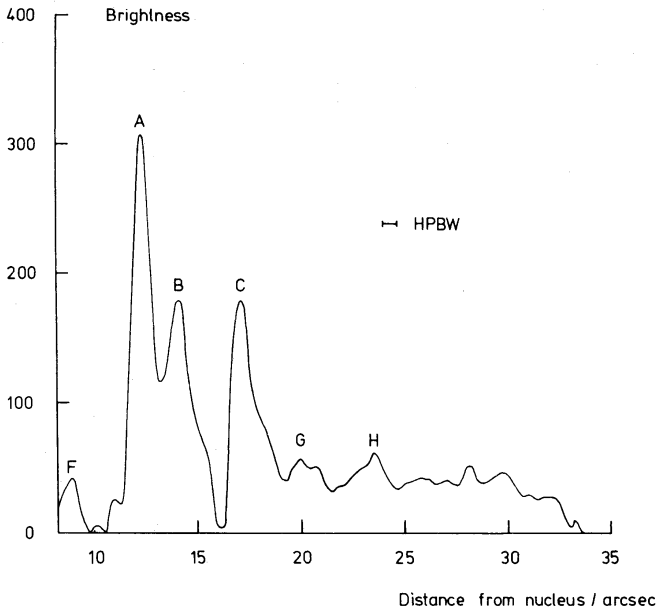

Figure 3. A brightness profile along the crest of the jet in M87 at 15.4 GHz. Brightness temperature (in arbitrary units) is plotted against distance from the nucleus.

Column 6: The apparent *B* magnitude of the knot (from VN).
Column 7: The peak flux density of the knot at 15.4 GHz.

Particularly interesting features of the brightness distribution are as follows:

(a) There are minima in the radio emission between F and A and between B and C where the surface brightness drops nearly to zero.

(b) The profile of knot C is peaked on the side nearer the nucleus. A and B may show similar behaviour, but the resolution is insufficient to make sure of this. The knots in the twin-tail source NGC 1265 (Owen, Burns & Rudnick 1978) are strikingly similar to those in the M87 jet.

(c) The surface brightness of the jet is relatively constant beyond C; local enhancements (for example G and H) are weak.

Table 1. Optical and radio parameters of the knots.

Knot		α(1950.0) h m s	±s	δ(1950.0) ° ′ ″	±″	θ/arcsec	B	±	S/mJy	±/mJy
D	Optical	12 28 17.378	0.009	12 40 02.76	0.13	-	18.25	0.20	-	-
E	Optical	17.17	0.07	03.7	1.0	-	19.20	0.20	-	-
F	Optical	17.034	0.016	04.83	0.24	0.7	18.60	0.20	40	10
	Radio	17.000	0.014	05.0	0.6					
A	Optical	16.775	0.011	06.21	0.16	0.9	16.70	0.05	300	15
	Radio	16.766	0.005	06.4	0.3					
B	Optical	16.642	0.019	07.09	0.28	1.5	17.35	0.05	180	10
	Radio	16.644	0.005	06.7	0.3					
C	Optical	16.439	0.025	08.14	0.37	1.2	17.48	0.05	180	10
	Radio	16.438	0.005	08.9	0.3					
G	Optical	16.278	0.018	09.17	0.26	1.4	19.35	0.15	60	10
	Radio	16.226	0.020	09.5	1.0					
H	Optical	15.99	0.07	08.9	1.0	1.2	20.90	0.40	60	10
	Radio	15.998	0.007	08.1	0.6					

(d) Both the jet and the diffuse structure in the western lobe show a sharp bend at RA $12^h\,28^m\,16^s.3$ (between C and G).

(e) Beyond G, the jet widens and merges into the surrounding emission. It is difficult to estimate the transverse size of the jet because of this lack of contrast; a rough value is $\theta \sim 3$ arcsec (300 pc) at and beyond H. Knots A, B and C are unresolved perpendicular to the jet axis, implying $\theta < 1$ arcsec.

The radio and optical brightness distributions are very similar in their region of overlap (Fig. 2); the diffuse emission beyond knot C is visible in both wavebands (Longair & Gunn, private communication). The knots which are detected at radio and at optical wavelengths are F, A, B, C, G and H; D and E are in a region of the radio map which is confused by residual sidelobes of the central source but are prominent in the optical waveband (Table 1) and are expected to produce radio emission. It is not clear whether I, J and K (see VN) are actually distinct features as they do not correspond to peaks in the radio emission in Fig. 2. The total projected length of the jet is 32 arcsec (3.1 kpc). It bends sharply and begins to fade and broaden at a distance of ~ 20 arcsec from the nucleus.

4 The magnetic field in the jet

4.1 OBSERVATIONS

A map of the western lobe of the source in which vectors representing the linearly-polarized intensity are superimposed on contours of total intensity, I, is shown in Fig. 4. The effects of Faraday rotation and depolarization are small; comparison with the polarization measurements of Turland (1975) at 5.0 GHz and Schmidt *et al.* (1978) at optical wavelengths suggest that for $\nu \geqslant 5$ GHz:

(a) depolarization of the radiation from the jet is negligible, and

(b) the Faraday rotation is consistent with a rotation measure of $+360\,\mathrm{rad\,m^{-2}}$, which is constant over the jet. The rotation introduced between infinite frequency and 15.4 GHz is therefore $+7^\circ.8$ and this value is unlikely to be in error by more than 2°.

Fig. 5 shows a map in which vectors whose lengths are proportional to the percentage polarization and whose directions are those of the projected *magnetic* field (corrected for Faraday rotation) are superimposed on a contour map of total intensity. The following features are immediately apparent:

(a) The field changes direction sharply on a scale of a few arcsec, but is always *parallel to the local axis of the jet.*

(b) The degree of polarization exceeds 30 per cent over much of the jet, indicating that the field is highly ordered (the theoretical maximum for the spectral index of the jet, $\alpha = 0.5$, is 69 per cent).

The degree of polarization found at 15.4 GHz is higher than that measured at optical wavelengths by Schmidt *et al.* (1978); this must be due entirely to the higher resolution of the present study, in which beam averaging is less important. The two minima in the percentage polarization in Fig. 5 (at the peak of knot C and between G and H) are attributable to averaging over regions in which the field direction changes by $\sim 90^\circ$.

An attempt to define the field direction over the whole of the jet is sketched in Fig. 6. The curve is tangential to the apparent magnetic field where its direction is known and is drawn along the crest of the jet. The field direction has been determined from Fig. 5

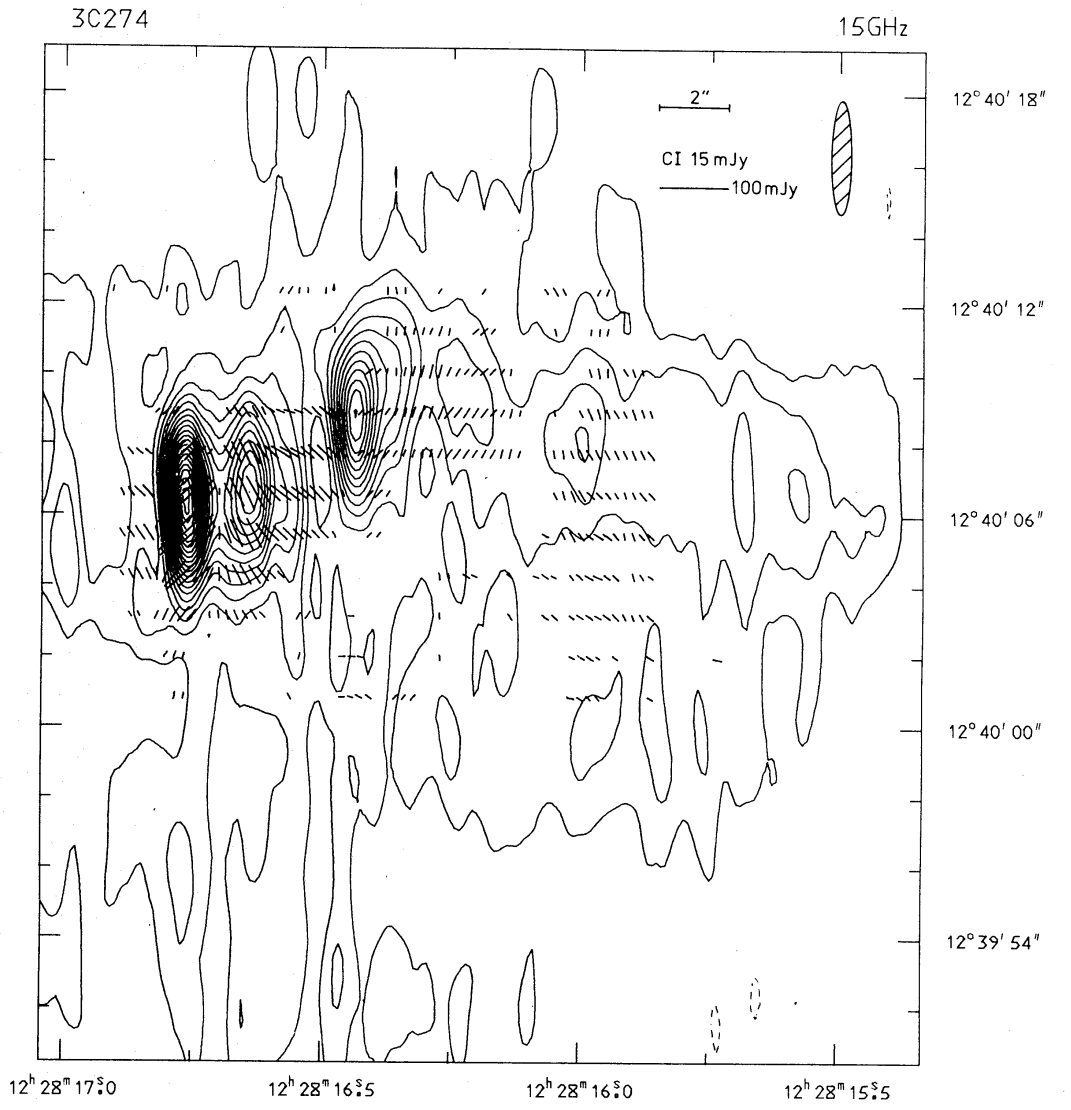

Figure 4. Vectors of linearly-polarized intensity superimposed on a contour map of total intensity for the western lobe of M87. The directions of the vectors are those of the *E*-vector of the polarized radiation. Vectors have only been plotted over the range of right ascension for which reliable measurements exist; those corresponding to a polarized flux density of less than 10 mJy have been omitted.

between A and H and from the optical polarization measurements of Schmidt *et al.* (1978) for D, E and F. Portions of the curve for which the field direction is unknown are drawn dotted and represent guesses at plausible directions.

The most natural explanation for the polarization structure is as follows:

(a) The jet oscillates from side to side with an amplitude which increases with increasing distance from the nucleus, as sketched in Fig. 6. The oscillation is quasi-periodic, with a wavelength of 3–4 arcsec (300–400 pc). Oscillations are also seen in the radio jets of 3C 31 (Burch 1979b), 3C 449 (Perley, Willis & Scott 1979), B0844 + 31 (van Breugel 1980) and NGC 6251 (Saunders, private communication).

(b) The magnetic field is aligned with the local axis of the jet and is highly ordered so that the degree of polarization averaged over a distance of ~ 1 arcsec (100 pc) is typically ~ 30 per cent.

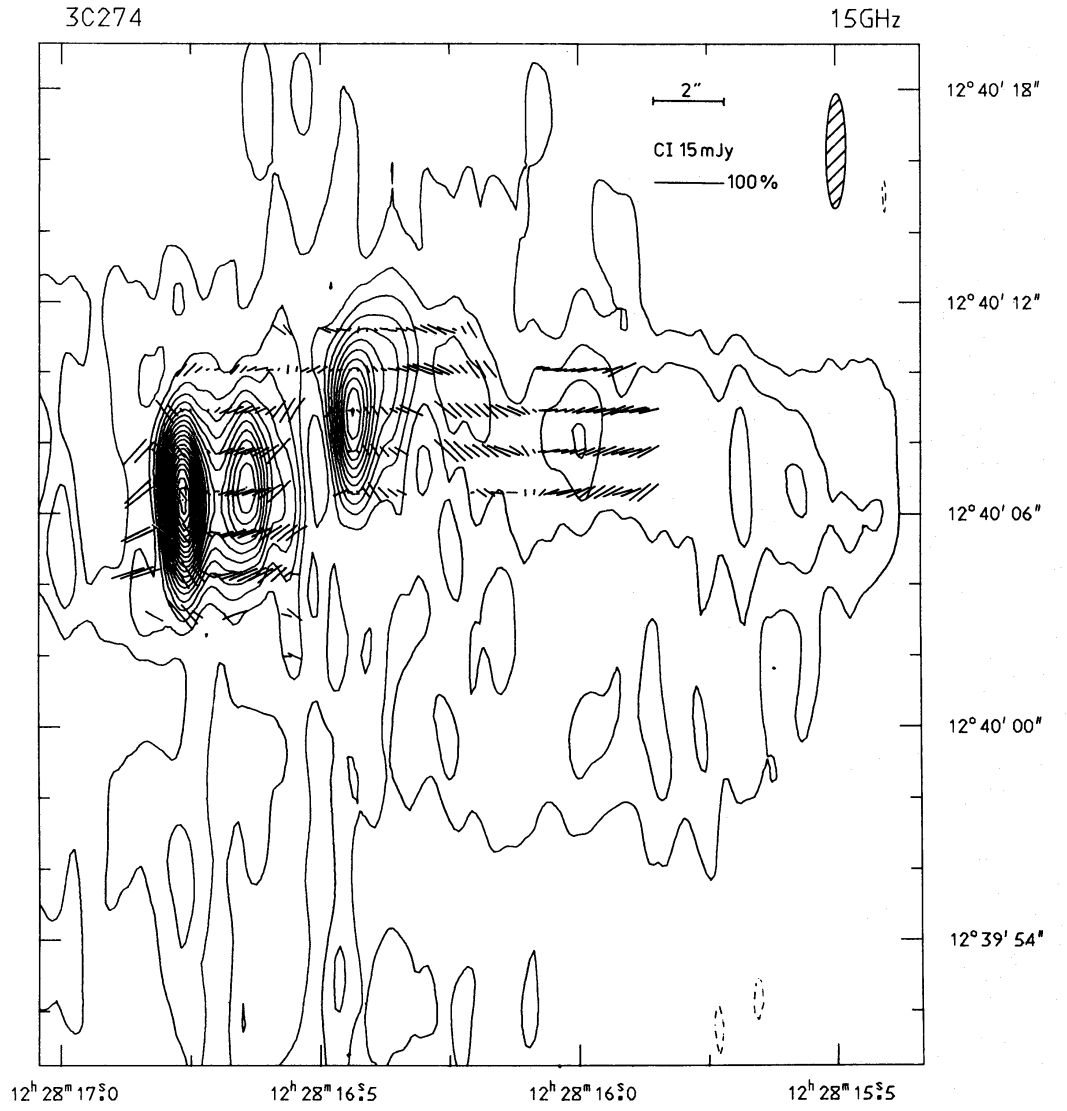

Figure 5. Vectors whose lengths are proportional to the percentage polarization and whose directions are those of the projected magnetic field superimposed on a contour map of total intensity. Vectors have only been plotted where the total intensity exceeds 25 mJy and where their directions are reliably determined.

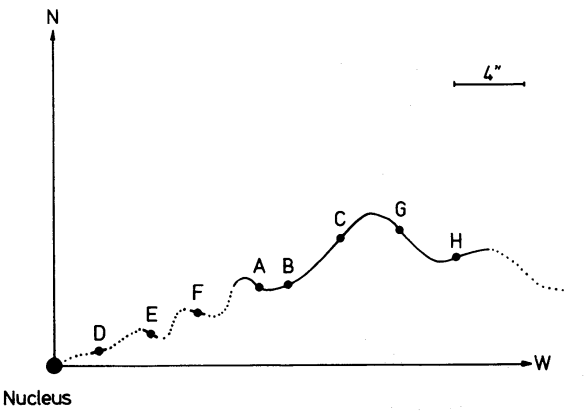

Figure 6. A sketch of the apparent magnetic field direction in the jet of M87. The curve is tangential to the field direction where this is known and is drawn along the crest of the jet. Dotted portions represent guesses at the field direction where this has not been measured.

4.2 COMPARISON WITH OTHER JETS

The extragalactic radio sources which have jets with well-determined apparent field directions are listed in Table 2, from which it can be seen that the fields are either parallel or perpendicular to the jet axes, no examples of intermediate orientations having yet been found. Three of the extended sources have parallel fields close to their nuclei, but perpendicular fields further out. Parallel fields seem to occur preferentially in the more powerful of the extended sources.

The jets in M87 and 3C 219 are alike in several respects: they consist of bright knots, are one-sided and have apparent magnetic fields which are parallel to their axes. A similar structure, this time double-sided, occurs in the twin-tail source NGC 1265 (Owen *et al.* 1978). One may speculate that knots are formed when jet is becoming unstable (for example by the pinching mode discussed by Hardee 1979) and are always associated with a field which is parallel to the axis of the jet.

Table 2. Apparent field directions in radio jets.

(a) Extended sources

Source	P_{178}/W Hz^{-1} sr^{-1}	Length of jet/kpc	Apparent field direction	References
3C 272.1 (M84)	6.4×10^{22}	6	Perpendicular	14
NGC 315	1.0×10^{24}	500	Parallel for 2 kpc, perpendicular after 13 kpc	3
3C 449	1.2×10^{24}	32	Perpendicular	12
3C 31	1.6×10^{24}	25	Parallel for 4.5 kpc, then perpendicular	5
NGC 6251	1.8×10^{24}	300	Parallel for 150 kpc, then perpendicular	10
3C 296	2.5×10^{24}	100	Perpendicular	2
3C 274 (M87)	6.6×10^{24}	3	Parallel	9
3C 219	4.4×10^{26}	76	Parallel	4,8,11
3C 273	5.6×10^{26}	20	Parallel	6
4C 32.69	1.2×10^{27}	180	Parallel	13

(b) Compact sources

3C 273	5.2×10^{26}	0.2	Parallel	7,15
3C 345	1.2×10^{27}	0.3	Parallel	7,15
3C 454.3	2.5×10^{27}	0.1	Parallel	7,15
3C 286	4.7×10^{27}	0.8	Perpendicular	9,15

References

1 This paper,
2 Birkinshaw, Laing & Peacock (in preparation),
3 Bridle *et al.* (1979),
4 Burch (1979a),
5 Burch (1979b),
6 Conway & Stannard (1972, 1975),
7 Davis, Stannard & Conway (1978),
8 Högbom (1979),
9 Laing (1980a),
10 Perley, quoted by Potash & Wardle (1980),
11 Perley *et al.* (1980),
12 Perley, Willis & Scott (1979),
13 Potash & Wardle (1980),
14 Riley (in preparation),
15 Wilkinson *et al.* (1979).

4.3 MODELS OF THE JET

Blandford & Königl (1979) identify the knots with dense clouds of gas which are confined and swept outwards by the ram pressure of a plasma jet. The radio emission is expected to come from the region of a strong shock behind the knot; the magnetic field in the emitting region should be predominantly parallel to the shock and wrapped around the knot (compare the model for the radio emission from the filaments of the Crab Nebula discussed by Laing (1980b) and Swinbank (1980)). The radio brightness distribution of a knot should then be elongated radially outwards from the nucleus of the galaxy and this disagrees with the results presented earlier. The observation that the projected magnetic field is aligned with the axis of a wavy jet also conflicts with the predictions of the model.

The model discussed by Rees (1978), in which the knots are interpreted as shocks caused by quasi-periodic variations in the velocity of a plasma beam, is consistent with the results presented here, but does not give a natural explanation for the oscillations of the jet.

Hardee (1979) suggests that the knots result from the hydrodynamic instabilities which are expected to perturb the surface of a jet and he shows that pinching and fluting modes are both important, although the former is likely to be dominant for a mildly supersonic jet. The oscillations in the jet may be attributable to the effects of instabilities and for this reason, the present observations seem to favour such a model.

5 Summary

The main conclusions of this work may be summarized as follows:

(a) The brightness distributions of the jet at optical and radio wavelengths are very similar.

(b) Within ~ 20 arcsec of the nucleus, the jet consists of sharp enhancements of emission (knots), at least some of which are peaked towards the nucleus, separated by regions of low surface brightness.

(c) At larger distances from the nucleus, the knots merge into a diffuse ridge of emission.

(d) The jet oscillates from side to side with a projected wavelength of 300–400 pc and an amplitude with increases with increasing distance from the nucleus.

(e) Observations of the linearly-polarized emission show that the magnetic field lies along the jet and faithfully follows its oscillations.

The oscillations and irregular emission in the jet strongly suggest a model in which a plasma beam supplying energy to the outer lobes has become unstable.

Acknowledgments

I am very grateful to John Baldwin and Peter Warner for their help with the data reduction and to Guy Pooley, Peter Scheuer and John Shakeshaft for their comments on the manuscript. I acknowledge financial support from the SRC and the Cavendish Laboratory.

References

Andernach, H., Baker, J. R., von Kap-Herr, A. & Wielebinski, R., 1979. *Astr. Astrophys.*, **74**, 93.
Blandford, R. D. & Königl, A., 1979. *Astrophys. Lett.*, **20**, 15.
Bridle, A. H., Davis, M. M., Fomalont, E. B. & Strom, R. G., 1979. *Astrophys. J.*, **228**, L9.

Burch, S. F., 1979a. *Mon. Not. R. astr. Soc.*, **186**, 519.
Burch, S. F., 1979b. *Mon. Not. R. astr. Soc.*, **187**, 187.
Conway, R. G. & Stannard, D., 1972. *Nature, Phys. Sci.*, **239**, 22.
Conway, R. G. & Stannard, D., 1975. *Nature*, **255**, 310.
Davis, R. J., Stannard, D. & Conway, R. G., 1978. *Mon. Not. R. astr. Soc.*, **185**, 435.
de Vaucouleurs, G. & Nieto, J.-L., 1979. *Astrophys. J.*, **231**, 364.
Forster, J. R., Dreher, J., Wright, M. C. H. & Welch, W. J., 1978. *Astrophys. J.*, **221**, L3.
Genzel, R., Pauliny-Toth, I. I. K., Preuss, E. & Witzel, A., 1976. *Astr. J.*, **81**, 1084.
Hardee, P. E., 1979. *Astrophys. J.*, **234**, 47.
Högbom, J. A., 1979. *Astr. Astrophys. Suppl.*, **36**, 173.
Kotanyi, C. G., 1980. *Astr. Astrophys.*, **83**, 245.
Laing, R. A., 1980a. *Mon. Not. R. astr. Soc.*, in press.
Laing, R. A., 1980b. *Mon. Not. R. astr. Soc.*, in press.
Owen, F. N., Burns, J. O. & Rudnick, L., 1978. *Astrophys. J.*, **226**, L119.
Perley, R. A., Bridle, A. H., Willis, A. G. & Fomalont, E. B., 1980. *Astr. J.*, **85**, 499.
Perley, R. A., Willis, A. G. & Scott, J. S., 1979. *Nature*, **281**, 473.
Potash, R. & Wardle, J. F. C., 1980. Preprint.
Riley, J. M. & Pooley, G. G., 1978. *Mon. Not. R. astr. Soc.*, **183**, 245.
Rees, M. J., 1978. *Mon. Not. R. astr. Soc.*, **184**, 61P.
Schmidt, G. D., Peterson, B. M. & Beaver, E. A., 1978. *Astrophys. J.*, **220**, L31.
Swinbank, E., 1980. *Mon. Not. R. astr. Soc.*, **193**, 451.
Tabara, H. & Inoue, M., 1980. *Astr. Astrophys. Suppl.*, **39**, 379.
Turland, B. D., 1975. *Mon. Not. R. astr. Soc.*, **170**, 281.
van Breugel, W. J. M., 1980. *Astr. Astrophys.*, **81**, 275.
Wilkinson, P. N., Readhead, A. C. S., Anderson, B. &. Purcell, G. H., 1979. *Astrophys. J.*, **232**, 365.